European Journal of Medicinal Chemistry 46 (2011) 756–764

Contents lists available at ScienceDirect

European Journal of Medicinal Chemistry

journal homepage: http://www.elsevier.com/locate/ejmech

Original article

HIV-1 integrase strand-transfer inhibitors: Design, synthesis and molecular modeling investigation

Laura De Luca [a,*], Sara De Grazia [a,*], Stefania Ferro [a,1], Rosaria Gitto [a,1], Frauke Christ [b,2], Zeger Debyser [b,2], Alba Chimirri [a,1]

[a] Dipartimento Farmco-Chimico, University of Messina, Viale Annunziata, I-98168 Messina, Italy
[b] Molecular Virology and Gene Therapy, Katholieke Universiteit Leuven and IRC KULAK, Kapucijnenvoer 33, B-3000 Leuven, Flanders, Belgium

ARTICLE INFO

Article history:
Received 5 November 2010
Received in revised form
7 December 2010
Accepted 11 December 2010
Available online 21 December 2010

Keywords:
HIV-1 integrase
INSTIs
PFV-IN/DNA
Benzylindoles
Molecular docking

ABSTRACT

This study is focused on a new series of benzylindole derivatives with various substituents at the benzene-fused ring, suggested by our 3D pharmacophore model developed for HIV-1 integrase inhibitors (INIs). All synthesized compounds proved to be active in the nanomolar range (6–35 nM) on the strand-transfer step (ST). In particular, derivative 4-[1-(4-fluorobenzyl)-5,7-dimethoxy-1*H*-indol-3-yl]-2-hydroxy-4-oxobut-2-enoic acid (**8e**), presenting the highest best-fit value on pharmacophore model, showed a potency comparable to that of clinical INSTIs GS 9137 (**1**) and MK-0518 (**2**). The binding mode of our molecules has been investigated using the recently published crystal structure of the complex of full-length integrase from the prototype foamy virus in complex with its cognate DNA (PFV-IN/DNA). The results highlighted the ability of derivative **8e** to assume the same binding mode of MK-0518 and GS 9137.

1. Introduction

It was recently reported that more than 33 million of people were infected worldwide with human immunodeficiency virus (HIV-1). The overall number of people living with HIV has increased as a result of new infections and the beneficial effects of the more widely available highly active anti-retroviral therapy (HAART), which employs a combinational use of drugs [1].

The currently FDA approved anti-HIV drugs belong to seven different groups: nucleoside reverse transcriptase inhibitors (NRTIs), nucleotide reverse transcriptase inhibitors (NtRTIs), non-nucleoside reverse transcriptase inhibitors (NNRTIs), protease inhibitors (PIs), fusion inhibitors (FIs), co-receptor inhibitors (CRIs) and integrase inhibitors (INIs) [2].

Although the HAART has brought about a substantial decrease in the death rate, changing AIDS from a rapidly lethal disease into a chronic manageable condition, the retroviral infection can be only temporarily controlled but not eradicated since HIV-1 becomes almost undetectable in the plasma for more than two years, persisting in *reservoirs*.

Furthermore the HAART efficacy has been limited by the emergence of drug-resistant viral strains, drug-toxicity, the poor ability of patients to adhere to the prescribed therapy and costs, so a refining of the current therapies and the developing of new therapeutic paradigms are still warranted [3]. Considering that HIV-IN plays a key role in stable infection and that, apart the RAG recombinases [4], there is no known human counterpart of HIV-IN it is understandable how this enzyme is an attractive therapeutic target.

HIV-1 IN, mechanistically and structurally, belongs to the superfamily of polynucleotidyl transferases, which includes the RNaseH and the transposases from Tn5. IN inserts a double-stranded DNA copy of the viral RNA genome into the chromosomes of an infected cell through a multistep process that involves two separate reactions. In the first step, termed 3′-processing, IN leads to the formation of new 3′-CA-OH. The second step, named strand-transfer (ST), is a trans-esterification reaction involving a direct nucleophilic attack of the 3′-hydroxy group of the two newly processed viral 3′-DNA ends on the phosphodiester backbone of the

Abbreviations: INSTIs, integrase strand transfer inhibitors; PFV, prototype foamy virus; DKAs, diketo acids; IFD, induced-fit docking.

* Corresponding authors. Fax: +39 090 355 613.
E-mail addresses: ldeluca@unime.it (L. De Luca), sdegrazia@pharma.unime.it (S. De Grazia), sferro@unime.it (S. Ferro), rgitto@unime.it (R. Gitto), frauke.christ@med.kuleuven.be (F. Christ), zeger.debyser@med.kuleuven.be (Z. Debyser), achimirri@unime.it (A. Chimirri).
[1] Fax: +39 090 355 613.
[2] Fax: +32 16 336 336.

0223-5234/$ – see front matter © 2010 Elsevier Masson SAS. All rights reserved.
doi:10.1016/j.ejmech.2010.12.012

host target DNA. The integration reaction is completed by the removal of the two unpaired nucleotides at the 5′-end of the viral DNA and by the repair of the single stranded gaps created between the viral and the target DNA [5,6]. No energy source (e.g., ATP) is needed for the integration reaction, and only divalent cations are required for catalytic activity. In particular, the two metal cofactors of HIV-IN are thought to both be Mg^{2+} ions under physiological conditions [7–9].

Among numerous attempts to identify new drugs active against HIV-IN, diketo acids (DKAs) and their analogs were the first derivatives displaying potent anti-retroviral activity via IN inhibition and several synthetic and biological studies have been reported [10,11]. It is believed that their IN-binding mechanism is connected to the presence of DKA pharmacophoric motif which could be involved in a functional sequestration of one or both divalent metal ions in the enzyme catalytic site to form a ligand-M^{2+}-IN complex. This would subsequently block the transition state of the IN-DNA complex by competing with the target DNA substrate, acting as an "interfacial inhibitor" [12].

The global research efforts to identify drugs that inhibit HIV integrase recently led to two new strand-transfer inhibitors (INSTIs) GS 9137 (**1**) and MK-0518 (**2**) (Fig. 1), which proved to be highly effective and well-tolerated [13] and to date compound **2** is the first drug (Isentress) active against IN enzyme, approved by the FDA [14].

In recent years also our research group has been engaged in the structure-function study of HIV-IN and in the development of new inhibitors. We reported ligand-based approaches useful to generate three-dimensional pharmacophore models for INSTIs which led to identify a series of benzylindoles as novel and potent IN inhibitors (e.g. compound **3**, CHI-1043, Fig. 1) [15–17].

In addition, considering that the structure of full-length retroviral HIV-1 integrase, either separately or in complex with DNA was lacking, we developed different approaches to build models of the full-length integrase-DNA complex and used the obtained results for the design of new potential INSTIs and the improvement of their activity [18–22].

But the *in silico* models could be not realistic, even if they gave us some right information regarding the mechanism of action and the binding modes of INSTIs. So, when finally in 2010 Hare et al. reported a crystal structure of full-length integrase from the prototype foamy virus in complex with its cognate DNA and the INSTIs **1** and **2** [23] we were particularly interested to compare their results with ours. This novel structural information is definitely a breakthrough in the field of IN research, since the disclosed complexes can be considered the best surrogate structures for reliably modeling the binding of these HIV-1 INIs.

Therefore, in the present study we report the rational design and expanded SAR investigation of new 4-[1-(4-fluorobenzyl)-dimethoxy-1*H*-indol-3-yl]-2-hydroxy-4-oxobut-2-enoic derivatives useful in clarifying the features important for ST inhibitors whereas the crystallographic data of PFV-IN complex were used to obtain more details about the binding mode of our new compounds in comparison with other well-known INSTIs.

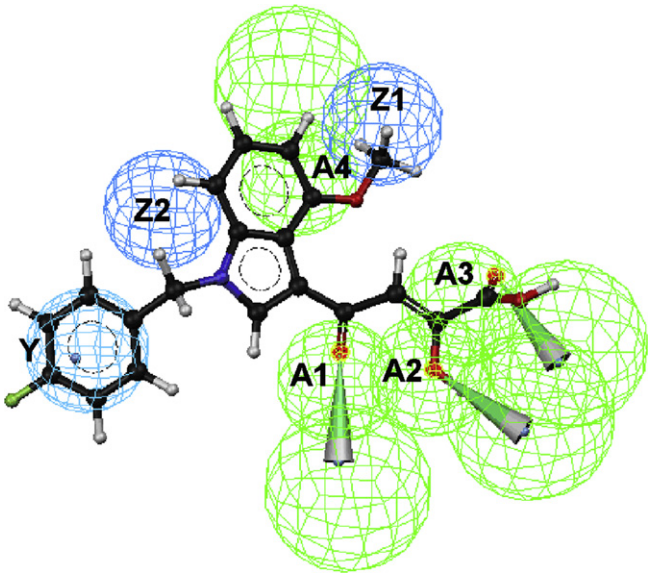

Fig. 2. Alignment of compound **3** into the pharmacophore model [17] (A1–A4, hydrogen-bond acceptor; Z1–Z2, hydrophobic aliphatic; Y, hydrophobic aromatic).

2. Results and discussion

DKA derivatives and their analogs which belong to the INSTIs represent the major leads in the development of anti-HIV-1 IN drugs. In fact, both **2** (Fig. 1) that is the only one drug approved by FDA and other potent IN inhibitors (i.e. **1**) are structurally related to the DKA family.

Our previously reported three-dimensional pharmacophore models allowed us the discovery of potent INSTIs (i.e. CHI-1043, **3** Fig. 1). The more recent of our pharmacophore models consisted of seven features, four hydrogen-bond acceptors (A1–A4), two hydrophobic aliphatic regions (Z1 and Z2) and one aromatic feature (Y). The overlapping of compound **3** onto our model is shown in Fig. 2. The β-diketo acid moiety maps the three hydrogen-bond acceptors (A1–A3), the *p*-fluorobenzyl ring overlaps the aromatic feature Y, and the 4-methoxy group occupies the aliphatic region Z1 whereas zone Z2 remained clear and taken together with our preliminary results this suggested that the introduction of an additional methoxy group at C-7 position should result in an improvement of inhibitory activity [17].

Taking into account these findings, in this work we focused our efforts to occupy all the pharmacophore model features by choosing to insert two methoxy groups in different positions of the benzene-fused ring of the indole nucleus and keeping unchanged the N-benzyl moiety of **3** (Fig. 2). So the synthesis of a new series of dimethoxy-*p*-fluoro-benzylindoles have been performed and the compounds obtained have been tested as IN inhibitors and anti-HIV agents.

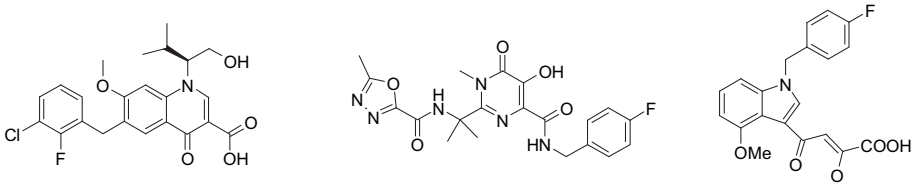

Fig. 1. HIV-1 integrase strand-transfer inhibitors.

2.1. Chemistry

The synthetic route employed to obtain the title compounds is depicted in Scheme 1.

Dimethoxyindoles **4a**–**f** were 3-acetylated by a Vilsmeier Haack reaction and N-alkylated by treatment with 4-fluorobenzyl bromide, in the presence of a catalytic amount of sodium hydride to give intermediates **6a**–**f**. Successively diketo esters **7a**–**f**, obtained by coupling with diethyl oxalate, were converted in the final derivatives **8a**–**f** by hydrolysis in basic medium. The preparation of commercially unavailable indoles **4a**, **4e**, and **4f** is shown in Schemes 2–4. The introduction of a nitro group on 2,3-dimethoxybenzaldehyde afforded a mixture of 5- and 6-nitro derivatives which were separated by flash chromatography on silica gel eluting with 30% EtOAc/cyclohexane [24]. The 2,3-dimethoxy-6-nitrobenzaldehyde was converted into the corresponding 2,3-dimethoxy-6,β-dinitrostyrene by refluxing with nitromethane in the presence of glacial acetic acid and ammonium acetate. Finally 4,5-dimethoxyindole (**4a**) was obtained by a Henry's reductive cyclization [25] (Scheme 2).

5,7-Dimethoxyindole (**4e**) was synthesized according with Condie's procedure, obtaining high yields. A solution of 3,5-dimethoxybenzaldehyde in nitromethane was refluxed to afford 3,5-dimethoxy-β-nitrostyrene which was converted in the nitro derivative and then into the desired product by reductive cyclization (Scheme 3) [26].

A different synthetic pathway, according to a modification of Rege's procedure, was followed to obtain the dimethoxy substitution at the 6-C and 7-C positions of the indole nucleus (Scheme 4).

The treatment of commercially available 3-methoxy-4-hydroxybenzaldehyde with acetic anhydride provided the *O*-acyl protected intermediate which, after nitration, was hydrolyzed under basic conditions. Methylation of the hydroxyl group with dimethyl sulfate followed by reaction with nitromethane and reductive cyclization as with the preparation of **4e**, gave 6,7-dimethoxyindole (**4f**) [27].

2.2. Biological activity

To determine the susceptibility of the HIV-1 integrase enzyme (Table 1) toward synthesized compounds **7a**–**f** and **8a**–**f**, we used enzyme-linked immunosorbent assays as described previously [28]. Moreover, their inhibitory effect on the HIV-1 induced cytopathic effect (CPE) in human lymphocyte MT-4 cell culture was determined by the MT-4/MTT-assay (Table 2) [29]. The biological results were compared with the data previously reported for indole derivative **3** and reference compounds **1**–**2**.

The biological assays revealed that the DKAs **8** exhibited inhibitory potency higher than the corresponding esters **7** with exception of ester derivative **7a** which was more active than the corresponding DKA **8a**. The analysis of biological results suggests that the introduction of an additional methoxy group at C-5 or C-7 position increases the IN-inhibitory effects. In fact, the disubstituted compounds **8a** and **8c** are more potent than the 4-monosubstituted derivative **3**. Moreover we found that the simultaneous presence of the methoxy substituent at 5 and 7 positions afforded the most potent INSTI of this series, the 4-[1-(4-fluorobenzyl)-5,7-dimethoxy-1*H*-indol-3-yl]-2-hydroxy-4-oxobut-2-enoic acid **8e**; it proved to be active at 6 nM concentration that is comparable to **2** (7 nM) and better than **1** (15 nM). On the contrary, the introduction of an additional methoxy group at C-6 seems to negatively influence the activity of this class of INSTIs (see compounds **8b**, **8d** and **8f**).

In the biological test against HIV-1 replication (Table 2), all DKAs **8a**–**f** showed EC_{50} values between 1.25 μM and 14.66 μM; they also proved to be better than corresponding esters **7a**–**f**. Compounds **8a** and **8c** displayed SI values (104 and 100, respectively) better than "lead compound" **3** (SI value of 70).

2.3. Computational studies

In order to explain the IN-inhibitory effects of the benzylindole derivatives we performed molecular modeling studies. All the scores for the ranking of the compounds in the pharmacophore model have been calculated (Supplementary data). Compound **8e**, that was the most active compound of the series, showed the best alignment (Fig. 3) in our pharmacophore model [17] further confirming its prediction power. Derivative **8e** (see Fig. 3) was able to perfectly occupy all the features of our model showing a high best-fit value (6.1). The two methoxy groups at C-5 and C-7 positions occupied both the hydrophobic areas Z1 and Z2; the β-diketo acid moiety fitted the three hydrogen-bond acceptors (A1–A3) whereas

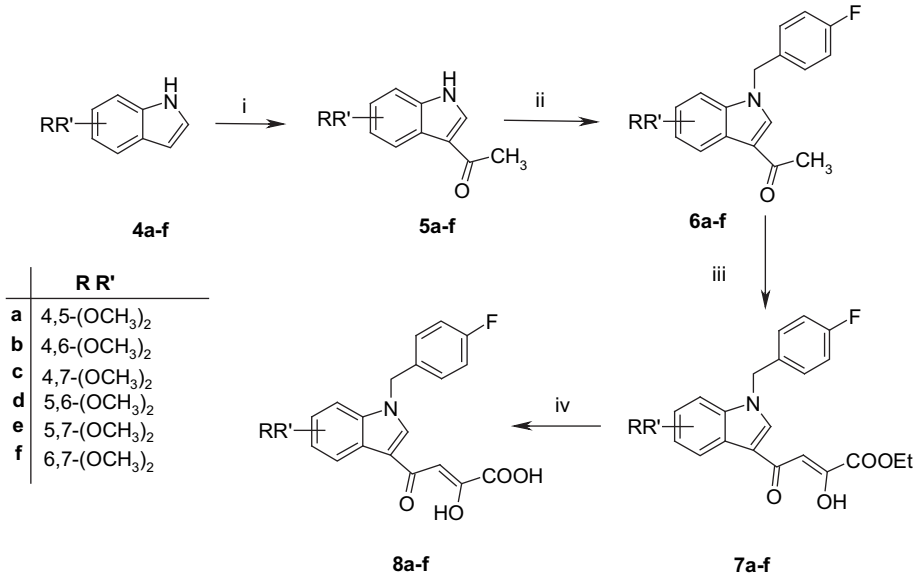

Scheme 1. Reagents and conditions: (i) $POCl_3$, $CH_3CON(CH_3)_2$, RT, 12 h; (ii) 4-fluorobenzyl bromide, NaH, DMF, mw: 5 min at continuous temperature (50 °C), 100 W; (iii) diethyl oxalate, dry CH_3ONa, THF, two separate steps under the same conditions mw: 2 min at continuous temperature (50 °C), 250 W; (iv) 2 N NaOH, MeOH, RT, 1.5 h.

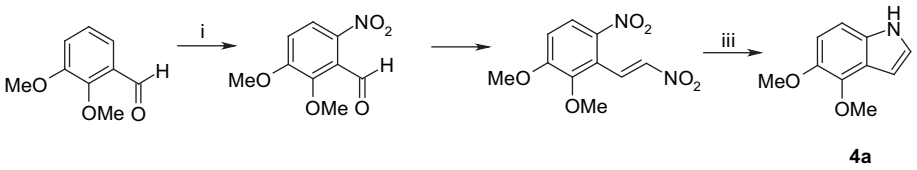

Scheme 2. Reagents and conditions: (i) glacial CH_3COOH 14 °C 10 min, fuming HNO_3, RT 1 h; (ii) CH_3NO_2, CH_3COONH_4, glacial CH_3COOH, Δ, 1.5 h; (iii) iron powder, glacial CH_3COOH, silica gel, toluene, Δ, 1.5 h.

the A4 region is occupied by the oxygen atom of the methoxy group in position 5 and *p*-fluorobenzyl ring matched the aromatic feature Y. With the aim to explore the main interactions with the target HIV-IN enzyme, we had already undertaken docking studies, when very interesting new data have been published [23]. In particular it has been demonstrated that the prototype foamy virus (PFV) IN was sensitive to HIV-1 INSTIs and the crystal structures of compounds **1** and **2** in complex with the full-length PFV IN and its DNA were solved [23].

These novel crystallographic data suggest an induced-fit mechanism of inhibition, where the halobenzyl groups of INSTIs fit into a pocket created by displacement of the terminal 3′-adenosine. These observations are in agreement with our induced-fit docking (IFD) procedure in which the 3′-terminal adenine nucleotide underwent a dramatic conformational movement in order to allow the insertion of the substituted benzyl moiety between the two viral DNA strands [20].

Therefore, with the aim to gain more information about the structure similarity of HIV-IN and PFV-IN, we decided to superimpose these two proteins using the core domain of PFV-IN complex with MK-0518 (**2**, Fig. 1) (pdb code 3L2T) [23] and the core domain of HIV-IN previously modeled by us (pdb code 1WKN) [18]. The results of this study are reported in Fig. 4.

As it is possible to note in the Fig. 4, there is a high similarity for the two 3D structures of integrases; the only significant difference is the orientation of the loop (residues 209–218 for PFV-IN and 140–149 for HIV-IN).

It has been previously reported the importance of the flexibility of this HIV-IN loop and the role of its residues associated with resistance to IN inhibitors. So, we concentrated our attention on the position of IN-PFV Tyr 212 residue (magenta stick style), corresponding to Tyr 143 of HIV-IN (green stick line), that is involved in stacking interactions with the inhibitor MK-0518 (**2**). In addition, the important part of conserved PFV-IN Pro 214 corresponding to HIV-IN Pro 145 highlighted the importance of this loop orientation for the binding mode of the INIs. So, considering crucial the orientation of the loop and the position of the side-chain of its residues for the interaction of INIs we decided to use the X-ray structure of integrase with DNA and two Mg ions from PFV-IN/MK-0518 complex (pdb code 3L2T) for docking studies of our compounds thus employing a realistic complex. Docking studies were performed using the GOLD program [30]. After the validation of the docking protocol (see Experimental section), compounds **7a**–**f** and **8a**–**f** were docked in the same binding site and the result of the most active compound of the series **8e** (yellow) was superimposed with the X-ray position of **1** (orange) and **2** (cyan), showing a similar binding mode (Fig. 5).

In particular the benzyl ring of the three compounds is placed in the same pocket in contact with viral DNA and all of three compounds are able to interact with Mg ions. The methoxy group at C-5 of **8e** is orientated in the same position of the methyloxadiazole moiety and isopropyl fragment of **1** and **2** respectively. In turn the 7-methoxy substituent of **8e** corresponds to the position of methoxy group of compound **1**.

In Fig. 5B it is shown the best docked conformation of compound **8e** after optimization of the complex using Macromodel software (see Experimental section for details) together with our simplified 3D pharmacophore model. The *p*-fluorobenzyl group (Y) interacts with the residues A17 and C16 of viral DNA and in particular the fluorine atom seems to establish Van der Waals interactions with conserved Gln 215, thus confirming the key role of the halogen atoms in INSTIs [31]. The diketo acid moiety (A1–A3) is able to interact with the two divalent ions in the active site whereas 5-methoxy (Z2) and 7-methoxy (Z1) groups are involved in hydrophobic interactions with Tyr 212 ad Pro 214 respectively.

3. Conclusion

In summary, most of the compounds synthesized exhibit high inhibitory potency against the IN enzyme both on over-all activity and ST step. In particular, the highest potency has been found for DKA derivative **8e**, which inhibited the ST step of IN at 6 nM concentration that is comparable to **2** (7 nM) and better than **1** (15 nM). Molecular modeling study, based on pharmacophore models, as well as docking results revealed that the investigated compounds show high binding similarity with clinical INSTIs **1** and **2**. Moreover, the key role of some structural requirements for binding between IN and STIs has been demonstrated.

4. Experimental section

4.1. Chemistry

All the microwave-assisted reactions were carried out in a CEM Focused Microwave Synthesis System, Model Discover, working at the power necessary for refluxing under atmospheric conditions (i.e. 250–300 W). Melting points were determined on a BUCHI Melting Point B-545 apparatus and are uncorrected. Elemental analyses (C, H, N) were carried out on a Carlo Erba Model 1106 Elemental Analyzer and the results are within ±0.4% of the

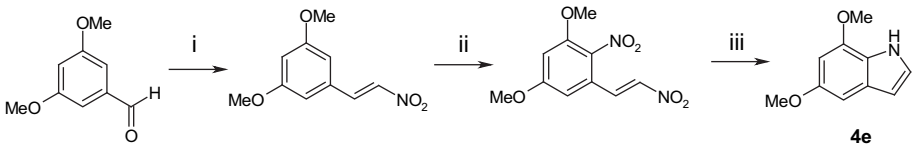

Scheme 3. Reagents and conditions: (i) CH_3NO_2, CH_3COONH_4, glacial CH_3COOH, Δ, 1.5 h; (ii) $Cu(NO_3)$, $(CH_3CO)_2O$, 60 °C, 2 h; (iii) iron powder, 80% aqueous CH_3COOH , 80°C-15 min, RT-1 h.

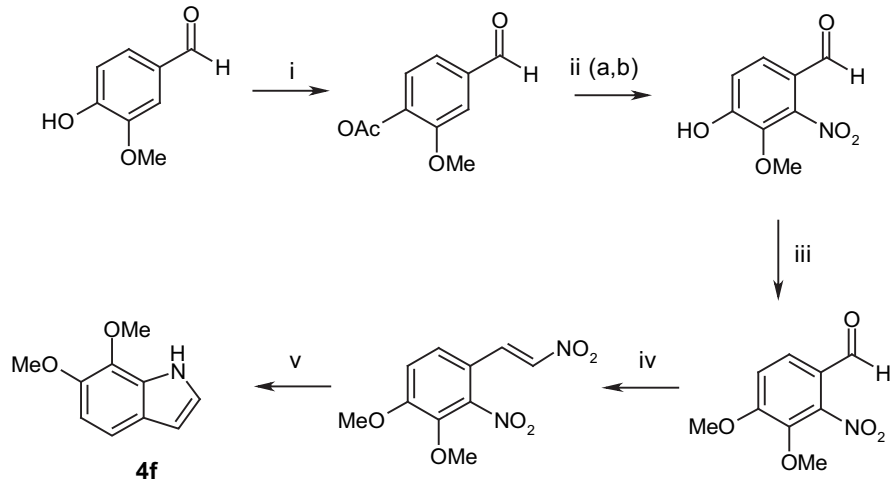

Scheme 4. Reagents and conditions: (i) Ac_2O, NEt_3, DMAP, rt, 3 h; (ii) a) fuming HNO_3, -10 °C, 4 h; b) 2 M KOH, Δ, 10 min; (iii) Me_2SO_4, absolute EtOH, 12 N NaOH, 50 °C, 3h; (iv) CH_3NO_2, CH_3COONH_4, glacial CH_3COOH, Δ, 1.5 h; (v) iron powder, glacial CH_3COOH, silica gel, toluene, Δ, 1.5 h.

theoretical values. Merck silica gel 60 F_{254} plates were used for analytical TLC; column chromatography was performed on Merck silica gel 60 (230–400 mesh) and Flash Chromatography (FC) on a Biotage SP_1 EXP. ^1H NMR spectra were recorded in $CDCl_3$ with TMS as internal standard or [D_6]DMSO on a Varian Gemini-300 spectrometer. Chemical shifts were expressed in δ (ppm) and coupling constants (*J*) in hertz. All the exchangeable protons were confirmed by addition of D_2O.

*4.1.1. General procedure for the synthesis of 3-acetyl-dimethoxy-1H-indoles (**5a**–**f**)*

Phosphoryl chloride (0.92 mL, 10 mmol) was added to ice cold dimethylacetamide (2.79 mL, 30 mmol) with stirring and cooling in ice. The suitable dimethoxyindole derivative (**4a**–**f**) (177 mg, 1 mmol) was added and reaction mixture was stirred at room temperature for 12 h, then poured over ice and basified with a 4 N aqueous sodium hydroxide solution. The mixture was extracted with ethyl acetate and dried over Na_2SO_4. After removal of the solvent under reduced pressure, the residue was powdered by treatment with diethyl ether and recrystallized from dichloromethane [31].

*4.1.1.1. 3-Acetyl-4,5-dimethoxy-1H-indole (**5a**).* White solid (166 mg, 76%): mp: 166–168 °C; ^1H NMR ($CDCl_3$): δ = 2.64 (s, 3H, CH_3), 3.93 (s, 3H, OCH_3), 3.95 (s, 3H, OCH_3), 7.00 (d, *J* = 8.6 Hz, 1H, ArH), 7.13 (d, *J* = 8.8 Hz, 1H, ArH), 7.83 (d, *J* = 2.7 Hz, 1H, ArH), 9.11 ppm (bs, 1H, NH); Anal. calcd for $C_{12}H_{13}NO_3$: C 65.74, H 5.98, N 6.39, found: C 65.85, H 5.71, N 6.51.

*4.1.1.2. 3-Acetyl-4,6-dimethoxy-1H-indole (**5b**).* White solid (101 mg, 46%): mp: 119–121 °C; ^1H NMR ([D_6]DMSO): δ = 2.46 (s, 3H, CH_3), 3.75 (s, 3H, OCH_3), 3.79 (s, 3H, OCH_3), 6.27 (d, *J* = 2.1 Hz, 1H, ArH), 6.51 (d, *J* = 1.9 Hz, 1H, ArH), 7.84 (s, 1H, ArH), 11.65 ppm (bs, 1H, NH); Anal. calcd for $C_{12}H_{13}NO_3$: C 65.74, H 5.98, N 6.39, found: C 65.83, H 6.21, N 6.51.

*4.1.1.3. 3-Acetyl-4,7-dimethoxy-1H-indole (**5c**).* Spectral data are in accordance with the literature [17].

*4.1.1.4. 3-Acetyl-5,6-dimethoxy-1H-indole (**5d**).* White solid (176 mg, 81%): mp: 147–149 °C; ^1H NMR ($CDCl_3$): δ = 2.53 (s, 3H, CH_3), 3.89 (s, 3H, OCH_3), 3.93 (s, 3H, OCH_3), 6.89 (s, 1H, ArH), 7.74 (d, *J* = 3.0 Hz, 1H,

Table 1
Inhibition of HIV-1 integrase activity.

Cpd	Over-all[a] IC_{50} (μM)	ST[b] C_{50} (μM)
7a	0.9 ± 0.36	0.015 ± 0.003
7b	2.79 ± 0.5	1.29 ± 0.64
7c	1.24 ± 0.06	0.66 ± 0.01
7d	4.4 ± 1.56	7.69 ± 1.43
7e	18.1 ± 3.5	34.9 ± 5.2
7f	7.41 ± 2.11	17.41 ± 10.05
8a	1.45 ± 0.46	0.047 ± 0.03
8b	0.47 ± 0.2	0.28 ± 0.06
8c[c]	0.06 ± 0.01	0.03 ± 0.01
8d	0.547 ± 0.15	0.119 ± 0.009
8e	0.251 ± 0.034	0.006 ± 0.003
8f	3.55 ± 3.78	6.37 ± 2.25
3	0.08 ± 0.003	0.14 ± 0.11
2	0.009 ± 0.0002	0.007 ± 0.0005
1	0.004 ± 0.003	0.015 ± 0.002

[a] Concentration required to inhibit the *in vitro* overall integrase activity by 50%.
[b] Concentration required to inhibit the *in vitro* strand-transfer step by 50%. All data represent average results ± SD.
[c] Data from Ref. [17].

Table 2
Activity in MT-4 cells.

Cpd	HIV-1[a] EC_{50} (μM)	Cytotoxicity[b] CC_{50} (μM)	SI[c]
7a	3.96 ± 0.63	111 ± 11	28
7b	2.48 ± 0.95	55.4 ± 2.35	22
7c[d]	4.09 ± 1.29	81.1 ± 5.68	20
7d	>21.76	21.76	<1
7e	>62.07	62.07	<1
7f	10.41 ± 3.46	119 ± 2.87	11
8a	1.21 ± 0.28	125.5 ± 5.5	104
8b	3.2 ± 0.97	20.7 ± 3.9	6
8c[d]	2.13 ± 0.05	213.3 ± 50.3	100
8d	10.52 ± 0.35	65.46 ± 2.97	6
8e	8.51 ± 0.32	58.5 ± 12.2	7
8f	14.66 ± 3.6	130.5 ± 12.5	9
3	0.59 ± 0.38	41.1 ± 16.7	70
2	0.013 ± 0.0005	>18	>1387
1	0.0008 ± 0.00009	2.12 ± 0.36	>2650

[a] Effective concentration required to reduce HIV-1-induced cytopathic effect by 50% in MT-4 cells.
[b] Cytotoxic concentration to reduce MT-4 cell viability by 50%.
[c] Selectivity index: ratio CC_{50}/EC_{50}. All data represent average results ± SD.
[d] Data from reference [17].

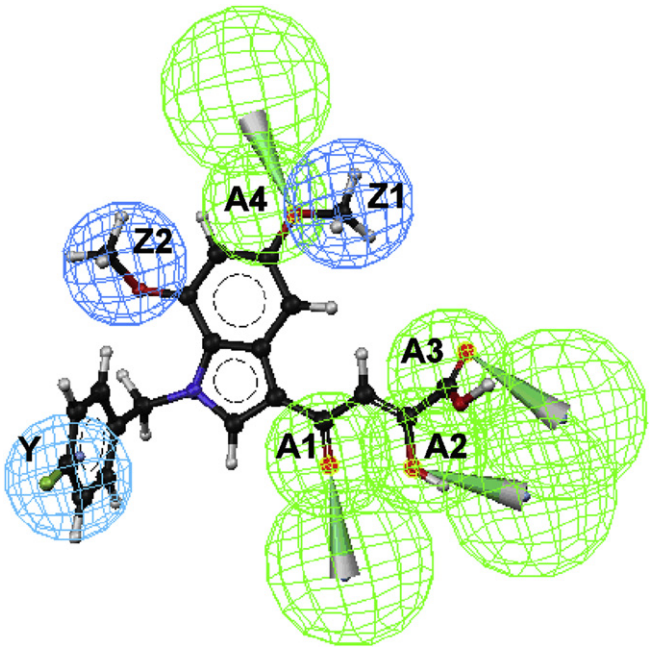

Fig. 3. Alignment of compound **8e** into pharmacophore model [17] (A1–A4, hydrogen-bond acceptor; Z1–Z2, hydrophobic aliphatic; Y, hydrophobic aromatic).

ArH), 7.89 (s, 1H, ArH), 8.71 ppm (bs, 1H, NH); Anal. calcd for $C_{12}H_{13}NO_3$: C 65.74, H 5.98, N 6.39, found: C 65.58, H 6.11, N 6.24.

*4.1.1.5. 3-Acetyl-5,7-dimethoxy-1H-indole (**5e**).* White solid (110 mg, 50%): mp: 198–200 °C; ^{1}H NMR ($CDCl_3$): $\delta = 2.52$ (s, 3H, CH_3), 3.89 (s, 3H, OCH_3), 3.92 (s, 3H, OCH_3), 6.41 (d, $J = 2.1$ Hz, 1H, ArH), 7.45 (d, $J = 2.1$ Hz, 1H, ArH), 7.76 (d, $J = 3.4$ Hz 1H, ArH), 8.76 ppm (bs, 1H, NH); Anal. calcd for $C_{12}H_{13}NO_3$: C 65.74, H 5.98, N 6.39, found: C 65.58, H 6.04, N 6.22.

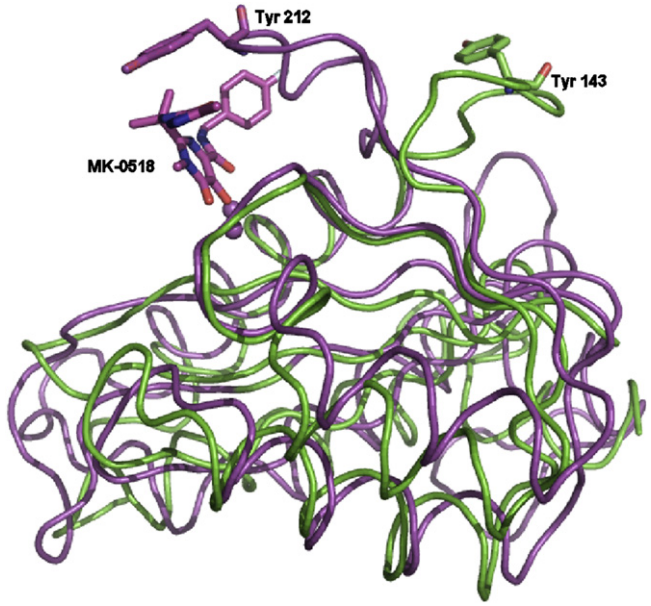

Fig. 4. Superimposed PFV-IN/2 complex (magenta) and HIV-IN (green). Compound MK-0518 (2), the residue Tyr 143 of HIV-IN and the corresponding Tyr 212 of PFV-IN are showed in stick line. This Figure was prepared using the PyMOL program [37]. (For interpretation of the references to colour in this figure legend, the reader is referred to the web version of this article.).

*4.1.1.6. 3-Acetyl-6,7-dimethoxy-1H-indole (**5f**).* White solid (212 mg, 97%): mp: 139–141 °C; ^{1}H NMR ($CDCl_3$): $\delta = 2.53$ (s, 3H, CH_3), 3.94 (s, 3H, OCH_3), 4.00 (s, 3H, OCH_3), 6.99 (d, $J = 8.8$ Hz, 1H, ArH), 7.78 (d, $J = 1.6$ Hz, 1H, ArH), 8.00 ppm (d, $J = 8.8$ Hz, 1H, ArH); Anal. calcd for $C_{12}H_{13}NO_3$: C 65.74, H 5.98, N 6.39, found: C 65.63, H 5.87, N 6.19.

*4.1.2. General procedure for the synthesis of 3-acetyl-dimethoxy-1-(4-fluorobenzyl)-1H-indoles (**6a–f**)*

The appropriate 3-acetyl-dimethoxy-1*H*-indole derivative (**5a–f**) (219 mg, 1 mmol) was dissolved in DMF (1 mL) at 0 °C and dry sodium hydride (120 mg, 5 mmol) was added. The mixture was stirred for 2 min. 4-fluorobenzyl bromide (283 mg, 1.5 mmol) was added dropwise and the resulting solution was placed in a cylindrical quartz tube (diam. 2 cm). The reaction mixture was then stirred and irradiated in a microwave oven at 100 W and at continuous temperature (50 °C) for 5 min. A saturated $NaHCO_3$ solution was added. The reaction mixture was extracted with ethyl acetate and dried over Na_2SO_4. After removal of the solvent under reduced pressure, the residue was powdered by treatment with diethyl ether and crystallized from a mixture of diethyl ether and dichloromethane [21].

*4.1.2.1. 3-Acetyl-4,5-dimethoxy-1-(4-fluorobenzyl)-1H-indole (**6a**).* Oil (255 mg, 78%); ^{1}H NMR ([D_6]DMSO): $\delta = 2.66$ (s, 3H, CH_3), 3.91 (s, 3H, OCH_3), 3.95 (s, 3H, OCH_3), 5.24 (s, 2H, CH_2), 6.92–7.16 (m, 6H, ArH), 7.75 ppm (s, 1H, ArH); Anal. calcd for $C_{19}H_{18}FNO_3$: C 69.71, H 5.54, N 4.28, found: C 69.63, H 5.61, N 4.47.

*4.1.2.2. 3-Acetyl-4,6-dimethoxy-1-(4-fluorobenzyl)-1H-indole (**6b**).* White solid (242 mg, 74%): mp: 102–104 °C; ^{1}H NMR ($CDCl_3$): $\delta = 2.64$ (s, 3H, CH_3), 3.78 (s, 3H, OCH_3), 3.94 (s, 3H, OCH_3), 5.21 (s, 2H, CH_2), 6.30 (d, $J = 1.9$ Hz, 1H, ArH), 6.35 (d, $J = 1.9$ Hz, 1H, ArH), 7.02–7.11 (m, 4H, ArH), 7.59 ppm (s, 1H, ArH); Anal. calcd for $C_{19}H_{18}FNO_3$: C 69.71, H 5.54, N 4.28, found: C 69.85, H 5.41, N 4.63.

*4.1.2.3. 3-Acetyl-4,7-dimethoxy-1-(4-fluorobenzyl)-1H-indole (**6c**).* Spectral data are in accordance with the literature [17].

*4.1.2.4. 3-Acetyl-5,6-dimethoxy-1-(4-fluorobenzyl)-1H-indole (**6d**).* White solid (219 mg, 67%): mp: 204–206 °C; ^{1}H NMR (CDCl3): $\delta = 2.53$ (s, 3H, CH_3), 3.89 (s, 3H, OCH_3), 4.03 (s, 3H, OCH_3), 5.33 (s, 2H, CH_2), 6.72 (s, 1H, ArH), 7.06–7.18 (m, 4H, ArH), 7.64 (s, 1H, ArH), 7.95 ppm (s, 1H, ArH); Anal. calcd for $C_{19}H_{18}FNO_3$: C 69.71, H 5.54, N 4.28, found: C 69.58, H 5.38, N 4.42.

*4.1.2.5. 3-Acetyl-5,7-dimethoxy-1-(4-fluorobenzyl)-1H-indole (**6e**).* White solid (196 mg, 60%): mp: 135–137 °C; ^{1}H NMR (CDCl3): $\delta = 2.47$ (s, 3H, CH_3), 3.80 (s, 3H, OCH_3), 3.89 (s, 3H, OCH_3), 5.55 (s, 2H, CH_2), 6.38 (d, $J = 2.1$ Hz, 1H, ArH), 6.99–7.09 (m, 4H, ArH), 7.51 (d, $J = 2.1$ Hz, 1H, ArH), 7.58 ppm (s, 1H, ArH); Anal. calcd for C19H18FNO3: C 69.71, H 5.54, N 4.28, found: C 69.63, H 6.12, N 4.37.

*4.1.2.6. 3-Acetyl-6,7-dimethoxy-1-(4-fluorobenzyl)-1H-indole (**6f**).* White solid (186 mg, 57%): mp: 122–124 °C; ^{1}H NMR ($CDCl_3$): $\delta = 2.48$ (s, 3H, CH_3), 3.68 (s, 3H, OCH_3), 3.91 (s, 3H, OCH_3), 5.57 (s, 2H, CH_2), 6.98–7.12 (m, 5H, ArH), 7.60 (s, 1H, ArH), 8.07 ppm (d, $J = 8.5$ Hz, 1H, ArH); Anal. calcd for $C_{19}H_{18}FNO_3$: C 69.71, H 5.54, N 4.28, found: C 69.81, H 6.02, N 4.11.

*4.1.3. General procedure for the synthesis of 4-[1-(4-fluorobenzyl)-dimethoxy-1H-indol-3-yl]-2-hydroxy-4-oxobut-2-enoates (**7a–f**)*

A mixture of suitable 3-acetyl-dimethoxy-1-(4-fluorobenzyl)-1*H*-indole (**6a–f**) (327 mg, 1 mmol) diethyl oxalate (219 mg, 1.5 mmol) and a catalytic amount of $NaOCH_3$ in anhydrous THF

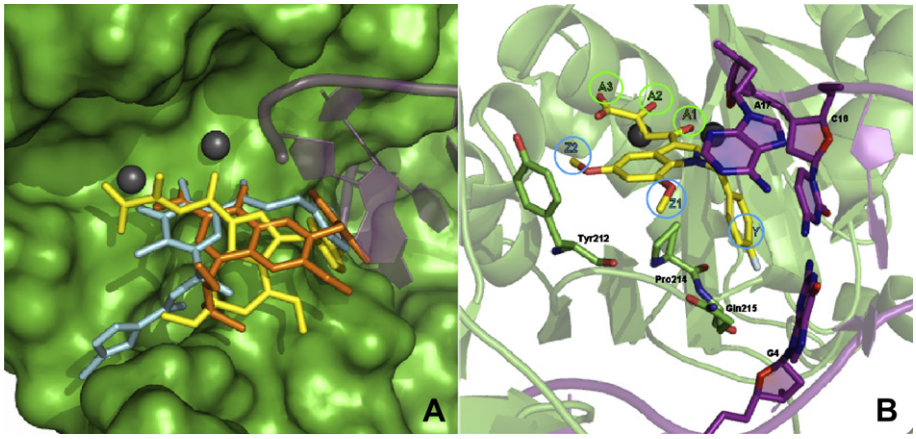

Fig. 5. (A) Docking pose of compound **8e** (yellow), compared to the crystallized position of 1 (orange) and 2 (cyan) in the IN-DNA active site. The divalent metal ions are shown as gray spheres, while the viral DNA is depicted in violet. (B) Docking pose of compound **8e** after minimization procedures. The colored spheres represented the 3D pharmacophore model developed by Catalyst. This Figure was prepared using the PyMOL program [37]. (For interpretation of the references to colour in this figure legend, the reader is referred to the web version of this article.).

(2 mL) was placed in a cylindrical quartz tube (diam. 2 cm), then stirred and irradiated at continuous temperature, in a microwave oven for two subsequent periods in the same conditions (250 W, 2 min, 50 °C). The solvent was evaporated under reduced pressure, the collected solid was washed with ether and crystallized from ethanol/diethyl ether. [21]

*4.1.3.1. Ethyl 4-[1-(4-fluorobenzyl)-4,5-dimethoxy-1H-indol-3-yl]-2-hydroxy-4-oxobut-2-enoate (**7a**).* Yellow solid (410 mg, 96%): mp: 213 °C dec; ^{1}H NMR ([D$_6$]DMSO): δ = 1.20 (t, J = 7.1 Hz, 3H, CH$_3$), 3.75 (s, 3H, OCH$_3$), 3.77 (s, 3H, OCH$_3$), 4.09 (q, J = 7.1 Hz, 2H, CH$_2$), 5.35 (s, 2H, CH$_2$), 6.47 (s, 1H, CH), 6.94 (d, J = 8.8 Hz, 1H, ArH), 7.11–7.17 (m, 3H, ArH), 7.25–7.30 (m, 2H, ArH), 7.80 ppm (s, 1H, ArH); Anal. calcd for C$_{23}$H$_{22}$FNO$_6$: C 64.63, H 5.19, N 3.28, found: C 64.72, H 5.22, N 3.39.

*4.1.3.2. Ethyl 4-[1-(4-fluorobenzyl)-4,6-dimethoxy-1H-indol-3-yl]-2-hydroxy-4-oxobut-2-enoate (**7b**).* Yellow solid (419 mg, 98%): mp: 110–112 °C; ^{1}H NMR ([D$_6$]DMSO): δ = 1.22 (t, J = 7.1 Hz, 3H, CH$_3$), 3.73 (s, 3H, OCH$_3$), 3.78 (s, 3H, OCH$_3$), 4.09 (q, J = 7.1 Hz, 2H, CH$_2$), 5.32 (s, 2H, CH$_2$), 6.23 (s, 1H, CH), 6.53–6.61 (m, 1H, ArH), 7.11–7.29 (m, 4H, ArH), 7.51 (d, J = 5.5 Hz, 1H, ArH), 8.50 ppm (s, 1H, ArH); Anal. calcd for C$_{23}$H$_{22}$FNO$_6$: C 64.63, H 5.19, N 3.28, found: C 64.48, H 5.37, N 3.38.

*4.1.3.3. Ethyl 4-[1-(4-fluorobenzyl)-4,7-dimethoxy-1H-indol-3-yl]-2-hydroxy-4-oxobut-2-enoate (**7c**).* Spectral data are in accordance with the literature [17].

*4.1.3.4. Ethyl 4-[1-(4-fluorobenzyl)-5,6-dimethoxy-1H-indol-3-yl]-2-hydroxy-4-oxobut-2-enoate (**7d**).* Yellow solid (384 mg, 90%): mp: 244 °C dec; ^{1}H NMR ([D$_6$]DMSO): δ = 1.32 (t, J = 7.1 Hz, 3H, CH$_3$), 3.82 (s, 6H, OCH$_3$), 4.19 (q, J = 7.1 Hz, 2H, CH$_2$), 5.47 (s, 2H, CH$_2$), 6.29 (s, 1H, CH), 7.15 (s, 1H, ArH), 7.20–7.26 (m, 2H, ArH), 7.39–7.43 (m, 2H, ArH), 7.95–7.98 ppm (m, 2H, ArH); Anal. calcd for C$_{23}$H$_{22}$FNO$_6$: C 64.63, H 5.19, N 3.28, found: C 64.51, H 5.27, N 3.11.

*4.1.3.5. Ethyl 4-[1-(4-fluorobenzyl)-5,7-dimethoxy-1H-indol-3-yl]-2-hydroxy-4-oxobut-2-enoate (**7e**).* Yellow solid (415 mg, 97%): mp: 110–112 °C; ^{1}H NMR ([D$_6$]DMSO): δ = 1.23 (t, J = 7.1 Hz, 3H, CH$_3$), 3.73 (s, 3H, OCH$_3$), 3.77 (s, 3H, OCH$_3$), 4.09 (q, J = 7.1 Hz, 2H, CH$_2$), 5.51 (s, 2H, CH$_2$), 6.17 (s, 1H, CH), 6.31 (d, J = 1.9 Hz, 1H, ArH), 7.08–7.52 (m, 5H, ArH), 8.49 ppm (s, 1H, ArH); Anal. calcd for C$_{23}$H$_{22}$FNO$_6$: C, 64.63; H 5.19, N 3.28, found: C 64.51, H 5.33, N 3.42.

*4.1.3.6. Ethyl 4-[1-(4-fluorobenzyl)-6,7-dimethoxy-1H-indol-3-yl]-2-hydroxy-4-oxobut-2-enoate (**7f**).* Yellow solid (419 mg, 98%): mp: 244 °C dec; ^{1}H NMR ([D$_6$]DMSO): δ = 1.23 (t, J = 7.1 Hz, 3H, CH$_3$), 3.60 (s, 3H, OCH$_3$), 3.79 (s, 3H, OCH$_3$), 4.09 (q, J = 7.1 Hz, 2H, CH$_2$), 5.52 (s, 2H, CH$_2$), 6.16 (s, 1H, CH), 6.91 (d, J = 8.8 Hz, 1H, ArH), 7.12 (d, J = 7.1 Hz, 2H, ArH), 7.89 (d, J = 6.3 Hz, 1H, ArH), 8.03 ppm (d, J = 9.1 Hz, 1H, ArH); Anal. calcd for C$_{23}$H$_{22}$FNO$_6$: C 64.63, H 5.19, N 3.28, found: C 64.47, H 5.06, N 3.11.

*4.1.4. General procedure for the synthesis of 4-[1-(4-fluorobenzyl)-dimethoxy-1H-indol-3-yl]-2-hydroxy-4-oxobut-2-enoic acids (**8a**–**f**)*

A methanol solution (5 mL) of derivatives **7a**–**f** (427 mg, 1 mmol) was treated with 2 N NaOH (5 mL, 50 mmol) and stirred at room temperature for 1.5 h. Then the reaction mixture was acidified with conc. HCl to afford a solid that was collected and recrystallized from ethanol/diethyl ether [21].

*4.1.4.1. 4-[1-(4-Fluorobenzyl)-4,5-dimethoxy-1H-indol-3-yl]-2-hydroxy-4-oxobut-2-enoic acid (**8a**).* Yellow solid (199 mg, 50%): mp: 120–122 °C; ^{1}H NMR ([D$_6$]DMSO): δ = 3.76 (s, 3H, OCH$_3$), 3.81 (s, 3H, OCH$_3$), 5.46 (s, 2H, CH$_2$), 7.08–7.19 (m, 3H, ArH e CH), 7.29–7.39 (m, 4H, ArH), 8.67 (s, 1H, ArH), 13.74 (bs, 1H, OH), 15.83 ppm (bs, 1H, OH); ^{13}C NMR ([D$_6$]DMSO): δ = 56.3, 56.7, 58.8, 104.8, 110.2, 111.1, 113.9, 115.4, 126.4, 129.7, 130.6, 131.8, 134.8, 146.5, 148.1, 159.9, 164.5, 187.6, 189.7 ppm; Anal. calcd for C$_{21}$H$_{18}$FNO$_6$: C 63.16, H 4.54, N 3.51, found: C 63.31, H 4.27, N 3.33.

*4.1.4.2. 4-[1-(4-Fluorobenzyl)-4,6-dimethoxy-1H-indol-3-yl]-2-hydroxy-4-oxobut-2-enoic acid (**8b**).* Yellow solid (199 mg, 50%): mp: 163–165 °C; ^{1}H NMR ([D$_6$]DMSO): δ = 3.76 (s, 3H, OCH$_3$), 3.86 (s, 3H, OCH$_3$), 5.45 (s, 2H, CH$_2$), 6.41 (s, 1H, CH), 6.76 (s, 1H, ArH), 7.17–7.37 (m, 5H, ArH), 8.39 ppm (s, 1H, ArH); ^{13}C NMR ([D$_6$]DMSO): δ = 55.8, 55.9, 58.8, 87.7, 88.2, 111.1, 113.9, 115.4, 117.8, 130.6, 131.8, 134.8, 138.3, 153.3, 154.7, 159.9, 164.5, 187.6, 189.7 ppm; Anal. calcd for C$_{21}$H$_{18}$FNO$_6$: C 63.16, H 4.54, N 3.51, found: C 63.27, H 4.71, N 3.64.

*4.1.4.3. 4-[1-(4-Fluorobenzyl)-4,7-dimethoxy-1H-indol-3-yl]-2-hydroxy-4-oxobut-2-enoic acid (**8c**).* Spectral data are in accordance with the literature. [17]

*4.1.4.4. 4-[1-(4-Fluorobenzyl)-5,6-dimethoxy-1H-indol-3-yl]-2-hydroxy-4-oxobut-2-enoic acid (**8d**).* Yellow solid (183 mg, 46%): mp: 193–195 °C; ^{1}H NMR ([D$_6$]DMSO): δ = 3.78 (s, 6H, OCH$_3$), 5.46 (s, 2H,

CH_2), 6.93 (s, 1H, CH), 7.14–7.20 (m, 2H, ArH), 7.25 (s, 1H, ArH), 7.42–7.46 (m, 2H, ArH), 7.69 (s, 1H, ArH), 8.77 ppm (s, 1H, ArH). ^{13}C NMR ([D_6]DMSO): δ = 56.3, 56.8, 58.8, 96.6, 103.4, 111.1, 113.9, 115.4, 119.4, 129.7, 130.6, 131.8, 134.8, 145.9, 148.1, 159.9, 164.5, 187.6, 189.7 ppm; Anal. calcd for $C_{21}H_{18}FNO_6$: C 63.16, H 4.54, N 3.51, found: C 63.27, H 4.39, N 3.40.

*4.1.4.5. 4-[1-(4-Fluorobenzyl)-5,7-dimethoxy-1H-indol-3-yl]-2-hydroxy-4-oxobut-2-enoic acid (**8e**).* Yellow solid (183 mg, 46%): mp: 175–177 °C; ^{1}H NMR ([D_6]DMSO): δ = 3.77 (s, 3H, OCH_3), 3.81 (s, 3H, OCH_3), 5.54 (s, 2H, CH_2), 6.45 (s, 1H, CH), 6.93 (s, 1H, ArH), 7.13–7.34 (m, 5H, ArH), 8.81 ppm (s, 1H, ArH). ^{13}C NMR ([D_6]DMSO): δ = 55.2, 55.8, 59.0, 85.6, 94.1, 111.1, 113.9, 115.4, 121.9, 128.6, 130.6, 131.8, 134.8, 147.8, 156.9, 159.9, 164.5, 187.6, 189.7 ppm; Anal. calcd for $C_{21}H_{18}FNO_6$: C 63.16, H 4.54, N 3.51, found: C 63.31, H 4.38, N 3.66.

*4.1.4.6. 4-[1-(4-Fluorobenzyl)-6,7-dimethoxy-1H-indol-3-yl]-2-hydroxy-4-oxobut-2-enoic acid (**8f**).* Yellow solid (176 mg, 44%): mp: 169–171 °C; ^{1}H NMR ([D_6]DMSO): δ = 3.63 (s, 3H, OCH_3), 3.82 (s, 3H, OCH_3), 5.55 (s, 2H, CH_2), 6.94 (s, 1H, CH), 7.08–7.21 (s, 5H, ArH), 7.92 (d, J = 8.5 Hz, 1H, ArH), 8.83 (s, 1H, ArH), 13.78 (bs, 1H, OH), 15.17 ppm (bs, 1H, OH). ^{13}C NMR ([D_6]DMSO): δ = 56.3, 56.8, 59.0, 111.1, 112.4, 112.9, 113.9, 115.4, 119.4, 130.0, 130.6, 131.8, 134.8, 137.5, 145.9, 159.9, 164.5, 187.6, 189.7 ppm; Anal. calcd for $C_{21}H_{18}FNO_6$: C 63.16, H 4.54, N 3.51, found: C 63.33, H 4.37, N 3.72.

4.2. Biological assays

4.2.1. Overall integrase assay using an enzyme-linked immunosorbent assay (ELISA)

To determine the susceptibility of the HIV-1 integrase enzyme toward different compounds we used enzyme-linked immunosorbent assays. These assays use an oligonucleotide substrate of which one oligonucleotide (5′-ACTGCTAGAGATTTTCCACACTGACTAAAAG-GGTC-3′) is labeled with biotin at the 3′ end and the other oligonucleotide is labeled with digoxigenin at the 5′ end. For the overall integration assay the second 5′-digoxigenin labeled oligonucleotide is (5′-GACCCTTTTAGTCAGTGTGGAAAATCTCTAGCAGT-3′). For the Strand Transfer assay the second oligonucleotide lacks GT at the 3′ end. The integrase enzyme was diluted in 750 mM NaCl, 10 mM Tris pH 7.6, 10% glycerol and 1 mM β-mercapto ethanol. To perform the reaction 4 μl diluted integrase (corresponding to a concentration of 1.6 μM) and 4 μl of annealed oligonucleotides (7 nM) was added in a final reaction volume of 40 μl containing 10 mM $MgCl_2$, 5 mM DTT, 20 mM HEPES pH 7.5, 5% PEG and 15% DMSO. The reaction was carried out for 1 h at 37 °C. Reaction products were denatured with 30 mM NaOH and detected by an immunosorbent assay on avidin coated plates. [32]

4.2.2. In vitro anti-HIV and drug susceptibility assays

The inhibitory effect of antiviral drugs on the HIV-induced cytopathic effect (CPE) in human lymphocyte MT-4 cell culture was determined by the MT-4/MTT-assay [29].

This assay is based on the reduction of the yellow colored 3-(4,5-dimethylthiazol-2-yl)-2,5-diphenyltetrazolium bromide (MTT) by mitochondrial dehydrogenase of metabolically active cells to a blue formazan derivative, which can be measured spectrophotometrically. The 50% cell culture infective dose ($CCID_{50}$) of the HIV(III_B) strain was determined by titration of the virus stock using MT-4 cells. For the drug-susceptibility assays, MT-4 cells were infected with 100–300 $CCID_{50}$ of the virus stock in the presence of five-fold serial dilutions of the antiviral drugs. The concentration of the various compounds that achieved 50% protection against the CPE of the different HIV strains, which is defined as the EC_{50}, was determined. In parallel the 50% cytotoxic concentration (CC_{50}) was determined.

4.3. Docking studies

The crystal structure of PFV-IN with DNA and two Mg ions complexed with the inhibitor **2** were retrieved from Protein Data Bank (pdb code 3L2T) and used for our modeling studies. Hydrogen atoms were added using the Schrodinger Maestro. The **2** structure was extracted from X-ray complex, and the other structures of the ligands were constructed using the Schrodinger Maestro [33], and were then submitted to Polak-Ribiere conjugate gradient minimization (0.0005 Kj/Å mol convergence). The compounds were presented in their enolic tautomeric form, since it has been clearly established that DKAs mainly exist in this form in solution, the carboxylic moiety was considered as carboxylate and the enolic oxygen as enolate given the influence of the two metal ions in the binding site [34]. The ligands minimized in this way were docked using GOLD 4.1.2 [30]. The region of interest used by Gold was defined in order to contain the residues within 15 Å from the original position of the ligand in the X-ray structures. CHEMPLP scoring function was chosen as the fitness function, default parameters were used and the ligands were submitted to 100 genetic algorithm runs.

Test docking calculation was carried out using compound **2** with the aim of comparing experimental and predicted binding modes and validating the docking protocol.

The best docking pose found for **2** agreed well with its experimental binding mode even if with root-mean square deviations (RMSD) of 1.13. This value can be due to the rotation, in the docking pose, of the oxadiazole ring where the two nitrogen atoms are oriented in opposite site with respect to X-ray position (see Supporting Information). In fact removing the methyloxadiazole group resulted in the RMSD value becoming 0.66.

4.4. Minimization process

All of PFV-IN/ligand complexes obtained by docking studies were minimized freezing the two cations and the 3′ OH oxygen, using 1000 iterations of SD and 1000 interaction of Polak-Ribiere Conjugate Gradient. Minimization of complexes was performed using OPLS-2005[35] force field and GB/SA model [36] as solvation treatment.

Acknowledgments

This work was supported by THINC project (European Commission HEALTH-F3-2008-201032).

Appendix. Supplementary data

Supplementary data associated with this article can be found, in the online version, at doi:10.1016/j.ejmech.2010.12.012.

References

[1] J.A. Este, T. Cihlar, Current status and challenges of antiretroviral research and therapy, Antiviral. Res. 85 (2010) 25–33.
[2] Y. Mehellou, E. De Clercq, Twenty-six years of anti-HIV drug discovery: where do we stand and where do we go? J. Med. Chem. 53 (2010) 521–538.
[3] M. Sechi, G. Rizzi, A. Bacchi, M. Carcelli, D. Rogolino, N. Pala, T.W. Sanchez, L. Taheri, R. Dayam, N. Neamati, Design and synthesis of novel dihydroquinoline-3-carboxylic acids as HIV-1 integrase inhibitors, Bioorg. Med. Chem. 17 (2009) 2925–2935.
[4] M. Melek, J.M. Jones, M.H. O'Dea, G. Pais, T.R. Burke Jr., Y. Pommier, N. Neamati, M. Gellert, Effect of HIV integrase inhibitors on the RAG1/2 recombinase, Proc. Natl. Acad. Sci. U.S.A. 99 (2002) 134–137.
[5] T.K. Chiu, D.R. Davies, Structure and function of HIV-1 integrase, Curr. Top. Med. Chem. 4 (2004) 965–977.
[6] V. Nair, G. Chi, R. Ptak, N. Neamati, HIV integrase inhibitors with nucleobase scaffolds: discovery of a highly potent anti-HIV agent, J. Med. Chem. 49 (2006) 445–447.

[7] J. d'Angelo, J.F. Mouscadet, D. Desmaele, F. Zouhiri, H. Leh, HIV-1 integrase: the next target for AIDS therapy? Pathol. Biol. (Paris) 49 (2001) 237–246.
[8] W. Yang, T.A. Steitz, Recombining the structures of HIV integrase, RuvC and RNase H, Structure 3 (1995) 131–134.
[9] O. Delelis, K. Carayon, A. Saib, E. Deprez, J.F. Mouscadet, Integrase and integration: biochemical activities of HIV-1 integrase, Retrovirology 5 (2008) 114.
[10] D.J. Hazuda, P. Felock, M. Witmer, A. Wolfe, K. Stillmock, J.A. Grobler, A. Espeseth, L. Gabryelski, W. Schleif, C. Blau, M.D. Miller, Inhibitors of strand transfer that prevent integration and inhibit HIV-1 replication in cells, Science 287 (2000) 646–650.
[11] A.A.M. Johnson, C. Pommier, HIV-1 IN inhibitors:a decade of research and two drugs in clinical trial, Curr. Top. Med. Chem. 4 (2004) 1059–1077.
[12] A. Bacchi, M. Biemmi, M. Carcelli, F. Carta, C. Compari, E. Fisicaro, D. Rogolino, M. Sechi, M. Sippel, C.A. Sotriffer, T.W. Sanchez, N. Neamati, From ligand to complexes. Part 2. Remarks on human immunodeficiency virus type 1 integrase inhibition by beta-diketo acid metal complexes, J. Med. Chem. 51 (2008) 7253–7264.
[13] J. Ramacharan, A.M. Skalka, Strategies for identification of HIV-1integrase inhibitors, Future Virol. 1 (2006) 717–731.
[14] www.fda.gov/bbs/topics/NEWS/2007/NEW01726.htmlin.
[15] M.L. Barreca, A. Rao, L. De Luca, M. Zappala, C. Gurnari, P. Monforte, E. De Clercq, B. Van Maele, Z. Debyser, M. Witvrouw, J.M. Briggs, A. Chimirri, Efficient 3D database screening for novel HIV-1 IN inhibitors, J. Chem. Inf. Comput. Sci. 44 (2004) 1450–1455.
[16] M.L. Barreca, S. Ferro, A. Rao, L. De Luca, M. Zappala, A.M. Monforte, Z. Debyser, M. Witvrouw, A. Chimirri, Pharmacophore-based design of HIV-1 integrase strand-transfer inhibitors, J. Med. Chem. 48 (2005) 7084–7088.
[17] L. De Luca, M.L. Barreca, S. Ferro, N. Iraci, M. Michiels, F. Christ, Z. Debyser, M. Witvrouw, A. Chimirri, A refined pharmacophore model for HIV-1 integrase inhibitors: optimization of potency in the 1H-benzylindole series, Bioorg. Med. Chem. Lett. 18 (2008) 2891–2895.
[18] L. De Luca, A. Pedretti, G. Vistoli, M.L. Barreca, L. Villa, P. Monforte, A. Chimirri, Analysis of the full-length integrase-DNA complex by a modified approach for DNA docking, Biochem. Biophys. Res. Commun. 310 (2003) 1083–1088.
[19] L. De Luca, G. Vistoli, A. Pedretti, M.L. Barreca, A. Chimirri, Molecular dynamics studies of the full-length integrase-DNA complex, Biochem. Biophys. Res. Commun. 336 (2005) 1010–1016.
[20] M.L. Barreca, N. Iraci, L. De Luca, A. Chimirri, Induced-fit docking approach provides insight into the binding mode and mechanism of action of HIV-1 integrase inhibitors, ChemMedChem. 4 (2009) 1446–1456.
[21] S. Ferro, L. De Luca, M.L. Barreca, N. Iraci, S. De Grazia, F. Christ, M. Witvrouw, Z. Debyser, A. Chimirri, Docking studies on a new human immunodeficiency virus integrase-Mg-DNA complex: phenyl ring exploration and synthesis of 1H-benzylindole derivatives through fluorine substitutions, J. Med. Chem. 52 (2009) 569–573.
[22] M.L. Barreca, F. Ortuso, N. Iraci, L. De Luca, S. Alcaro, A. Chimirri, Tn5 transposase as a useful platform to simulate HIV-1 integrase inhibitor binding mode, Biochem. Biophys. Res. Commun. 363 (2007) 554–560.
[23] S. Hare, S.S. Gupta, E. Valkov, A. Engelman, P. Cherepanov, Retroviral intasome assembly and inhibition of DNA strand transfer, Nature 464 (2010) 232–236.
[24] Y.I. Fukuyama, C. Kodama, M. Ochi, M. Kataoka, K. Shibata, Antimicrobial indolequinones from the mid-intestinal gland of the muricid gastropod Drupella fragum, Tetrahedron 54 (1998) 10007–10016.
[25] L. Henry, C.R. Hebd. Acad. Sci. 120 (1895) 1265–1268.
[26] G.C. Condie, M.F. Channon, A.J. Ivory, N. Kumar, D.St.C. Black, Regioselective reactivity of some 5,7-dimethoxyindoles, Tetrahedron 61 (2005) 4989–5004.
[27] P.D. Rege, Y. Tian, E.J. Corey, Studies of new indole alkaloid coupling methods for the synthesis of haplophytine, Org. Lett. 8 (2006) 3117–3120.
[28] K. Busschots, A. Voet, M. De Maeyer, J.C. Rain, S. Emiliani, R. Benarous, L. Desender, Z. Debyser, F. Christ, Identification of the LEDGF/p75 binding site in HIV-1 integrase, J. Mol. Biol. 365 (2007) 1480–1492.
[29] R. Pauwels, J. Balzarini, M. Baba, R. Snoeck, D. Schols, P. Herdewijn, J. Desmyter, E. De Clercq, Rapid and automated tetrazolium-based colorimetric assay for the detection of anti-HIV compounds, J. Virol. Methods 20 (1988) 309–321.
[30] GOLD 4.1.2; Cambridge Crystallographic Data Center: Cambridge CB2 1EZ, UK.
[31] S. Ferro, L. De Luca, M.L. Barreca, S. De Grazia, F. Christ, Z. Debyser, A. Chimirri, New chloro, fluorobenzylindole derivatives as integrase strand-transfer inhibitors (INSTIs) and their mode of action, Bioorg. Med. Chem. 18 (2010) 5510–5518.
[32] Y. Hwang, D. Rhodes, F. Bushman, Rapid microtiter assays for poxvirus topoisomerase, mammalian type IB topoisomerase and HIV-1 integrase: application to inhibitor isolation, Nucleic Acids Res. 28 (2000) 4884–4892.
[33] Maestro, Version 8.0. Schrodinger, LLC, New York, NY, 2007.
[34] C. Maurin, F. Bailly, E. Buisine, H. Vezin, G. Mbemba, J.F. Mouscadet, P. Cotelle, Spectroscopic studies of diketoacids-metal interactions. A probing tool for the pharmacophoric intermetallic distance in the HIV-1 integrase active site, J. Med. Chem. 47 (2004) 5583–5586.
[35] W.L.M. Jorgensen, D.S. Maxwell, J. Tirado-Rives, Development and testing of the OPLS all-atom force field on conformational energetics and properties of organic liquids, J. Am. Chem. Soc. 118 (1996) 11225–11236.
[36] W.C. Still, A. Tempczyk, R.C. Hawley, T. Hendrickson, Semianalytical treatment of solvation for molecular mechanics and dynamics, J. Am. Chem. Soc. 112 (1990) 6127–6129.
[37] W.L. DeLano, The PyMOL Molecular Graphics System. DeLano Scientific LLC, San Carlos, CA, USA., Available from http://www.pymol.org/.